Tooth Segmentation of Dental Study Models Using Range Images

Article *in* IEEE Transactions on Medical Imaging · April 2004

DOI: 10.1109/TMI.2004.824235 · Source: PubMed

3 authors:

Toshiaki Kondo
Thammasat University
89 PUBLICATIONS **409** CITATIONS
SEE PROFILE

Sim Heng Ong
National University of Singapore
276 PUBLICATIONS **3,918** CITATIONS
SEE PROFILE

Kelvin W. C. Foong
National University of Singapore
97 PUBLICATIONS **1,056** CITATIONS
SEE PROFILE

Tooth Segmentation of Dental Study Models Using Range Images

Toshiaki Kondo, S. H. Ong*, and Kelvin W. C. Foong

***Abstract*—The accurate segmentation of the teeth from the digitized representation of a dental study model is an important component in computer-based algorithms for orthodontic feature detection and measurement and in the simulation of orthodontic procedures such as tooth rearrangement. This paper presents an automated method for tooth segmentation from the three-dimensional (3-D) digitized image captured by a laser scanner. We avoid the complexity of directly processing 3-D mesh data by proposing the innovative idea of detecting features on two range images computed from the 3-D image. The dental arch is first obtained from the plan-view range image. Using the arch as the reference, a panoramic range image of the dental model can be computed. The interstices between the teeth are detected separately in the two range images, and results from both views are combined for a determination of interstice locations and orientations. Finally, the teeth are separated from the gums by delineating the gum margin. The algorithm was tested on 34 dental models representing a variety of malocclusions and was found to be robust and accurate.**

***Index Terms*—Dental arch, dental study model, range image, segmentation.**

I. Introduction

In recent years, much effort has been expended in developing computerized systems for clinical and research applications in dentistry. An expert system for automatic diagnosis in orthodontics[1] is described in [1]–[3]. Computer-aided design (CAD) and computer-aided manufacturing (CAM) in dentistry are examples of the introduction of computer technology to dentistry with successful clinical applications [4]–[9]. One such application is the automatic manufacturing of dental fillings such as crowns and inlays [4]. Computer-assisted design and fabrication of dental restorations have been proposed to speed production, eliminate labor-intensive steps, and provide consistent quality [5]. Presurgery simulation systems have been implemented for procedures such as tooth rearrangement and quantitative evaluation of three-dimensional (3-D) tooth movement [8], [9].

Tooth segmentation is an important step in many automated and semi-automated computer-based systems that require the accurate demarcation of individual teeth prior to the detection and measurement of dental features. Applications include the measurement of orthodontic parameters [1]–[3], simulation of tooth rearrangement for correction of malocclusion[2] [10], and pose estimation of teeth [11]. In an early attempt at tooth segmentation [1]–[3], the interstices (contact areas) between the teeth are detected along the U-shaped axis of a dental wax imprint [1], [2]. Orthodontic features such as the cutting edges of the incisors, tips of the cuspids (canines), and cusps[3] of the bicuspids (premolars) and molars are located using the watershed algorithm [3]. However, this system is not designed to deal with severe malocclusions but is targeted at the mild cases that are more likely to be encountered in epidemiological studies. In a recent work on tooth segmentation, line segments are detected using the Sobel filter and the completion to a closed contour is achieved by dynamic programming [4]. Since the authors are concerned with the restoration of the occlusal (biting) surfaces of the teeth, their work is limited to the posterior (back) teeth.

The above approaches to tooth segmentation, which make use of only the plan-view range image of the teeth, have had limited success due to the small incisor interstices and the deep fissures on the occlusal (biting) surface of the molars. An attempt to segment the teeth by processing a wire frame model is reported in [12] and [13], but only preliminary results using a few models are given. Similar to [1]–[3], this system is only designed to handle cases of mild malocclusion. Tooth segmentation is in general a difficult task because teeth come in different shapes and their arrangements vary substantially from one individual to another. The difficulty is exacerbated when the teeth are malaligned, which is a common occurrence in clinical cases.

In this paper, we present an automated method for segmenting the teeth of dental study models (plaster casts of the dentition) exhibiting a variety of malocclusions. Fig. 1 shows the overall flow diagram of the method. We digitize the model by surface scanning with a laser (Section II-A). After aligning the acquired image to a standard orientation (Section II-B), we generate a plan-view range image (Section II-B). Orthodontic features are extracted in this range image (Section III-A and Section III-B) for the determination of the dental arch (Section III-B). Using the arch as the reference, we generate a panoramic range image that provides a complete outer view of the cast, i.e., the entire buccal[4] surfaces of the teeth (Section III-C). The interstices between the teeth are detected separately in the two range images

Manuscript received May 31, 2003; revised November 4, 2003. The Associate Editor responsible for coordinating the review of this paper and recommending its publication was M. Sonka. *Asterisk indicates corresponding author.*

T. Kondo is with the Department of Electrical and Computer Engineering, National University of Singapore, Singapore 119260 Singapore.

*S. H. Ong is with the Department of Electrical and Computer Engineering, and the Division of Bioengineering, National University of Singapore, 10 Kent Ridge Crescent, Singapore 119260 Singapore (e-mail: eleongsh@nus.edu.sg).

K. W. C. Foong is with the Department of Preventive Dentistry, National University of Singapore, Singapore 119260 Singapore.

Digital Object Identifier 10.1109/TMI.2004.824235

[1]The dental specialty and practice of preventing and correcting irregularities of the teeth.

[2]Misalignment or faulty contact between the upper and lower teeth when the jaw is closed.

[3]The high points on the occlusal (biting) surfaces of the posterior (back) teeth.

[4]The outer surfaces of the teeth, i.e., tooth surfaces that are next to the cheeks (*opp.* lingual).

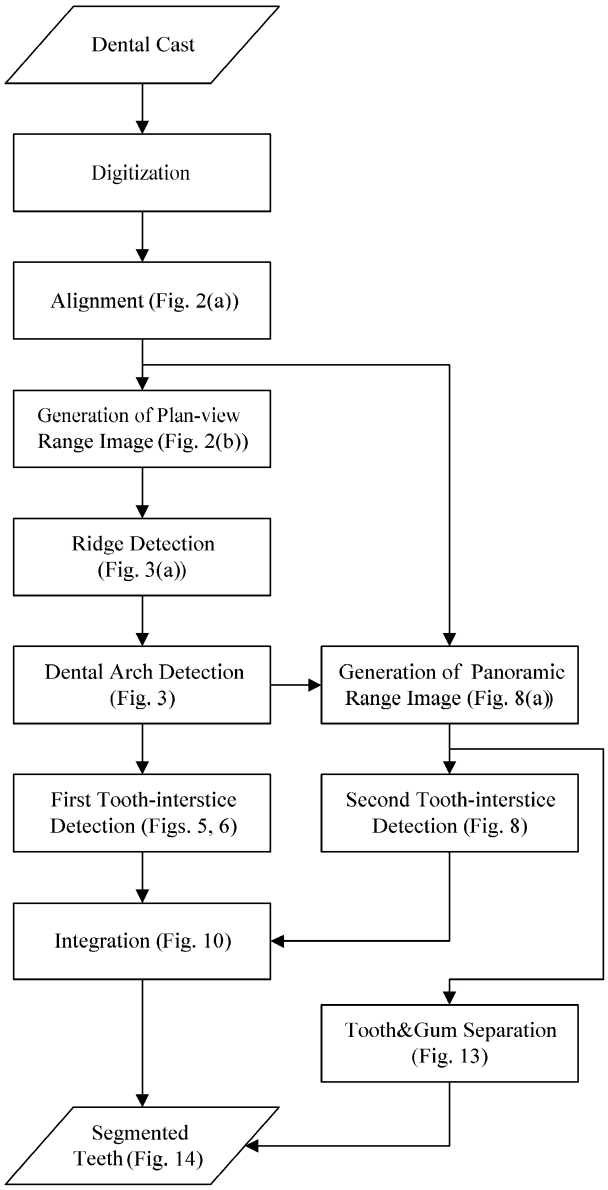

Fig. 1. Flow chart giving an overview of the segmentation procedure.

(Section IV-A and Section IV-B). The two results are subsequently combined to determine the position and the orientation of the tooth interstices (Section IV-C). Finally, the teeth are separated from the gums in the panoramic range image (Section IV-D). A validation test confirms that the method works well with dental casts representing a variety of malocclusions.

II. Data Acquisition and Processing

A. Data Acquisition

A variety of methods for acquiring digital data of the dentition have been reported in the literature. The 3-D profile of wax imprints can be obtained using a depth-from-absorption technique [1]–[3]. Range scanners have been used to scan dental study models for display and storage purposes [14]–[16]. A different approach that reconstructs the 3-D model of the patient's dental occlusion by integrating a sequence of images captured by an intraoral video camera is reported in [17].

We digitize the dental study models with a commercially available laser scanner (Cyberware 3030R/HIREZ/MM[5]) that provides high resolution and ease of use. A vertical strip of laser light is projected onto the plaster cast that is placed on the motion platform. As the object moves laterally, it is scanned by the stationary laser beam, and this is repeated for different rotated positions. Range information is computed from each scan. The bundled software produces the complete 3-D representation of the model by merging the range data from different scans. Spatial resolution is 0.15–1.00 mm horizontally and 0.30 mm vertically. Depth resolution depends on the surface quality of the object, but is typically 0.05–0.20 mm.

The 3-D image data is stored as a VRML file, in which an object is described as a list of vertices and a list of face indices. While this format is fine for visualization and data storage, it is not suitable for analysis because the vertices are listed in an irregular manner. There is also the inherent added complexity of working in the 3-D domain compared to two-dimensional (2-D) . Thus, instead of processing the VRML data directly, we devise algorithms that are applied to the range images (also called depth maps) generated from the 3-D data. A range image here is an array of pixels where each pixel value (gray level) represents the height of a sample point on the object from the reference surface. Since the range image is a 2-D matrix (though it has 3-D information encoded in the intensity values), the complex 3-D tooth segmentation problem is significantly simplified. We employ both plan-view and panoramic range images to provide the 3-D information necessary for tooth segmentation. It should also be noted that the image size is about 100 KB, which contrasts with 10 MB for the original mesh data.

B. Plan-View Range Image

In preparation for computing the plan-view range image, the digitized dental model has to be aligned to a standard orientation. We first specify the occlusal plane (the imaginary surface at which the upper and lower teeth touch) by manually identifying four reference points [Fig. 2(a)]: the disto-buccal[6] cusps of the first molars (labeled 1 and 4) and the buccal cusps of the first premolars (2 and 3). A reference point need not be precisely located as the program searches for the highest point in the vicinity of the manually selected point. The cast is aligned such that the occlusal plane is parallel to the x-y plane and the two disto-buccal cusps have the same y-coordinates. A plan-view range image is obtained [Fig. 2(b)] by mapping the vertices of the 3-D data onto a regularly spaced 2-D array. The image is made up of 300 by 300 pixels with each pixel corresponding to a spatial separation of $1/3$ mm. The highest 15-mm of the 3-D data is quantized into 256 gray levels, giving a height resolution of 0.059 mm per gray level. It is pertinent to note that the spatial and height resolutions of the range image are comparable to those of the scanner, thus ensuring the preservation of fine details in the conversion process.

III. Dental Arch Detection

In orthodontics, a complete description of the form of the dental arch is essential whenever changes due to growth or orthodontic therapies are under investigation [18]. Orthodontists

[5]http://www.cyberware.com.

[6]Posterior, i.e., toward the back of the mouth (*opp.*mesio-).

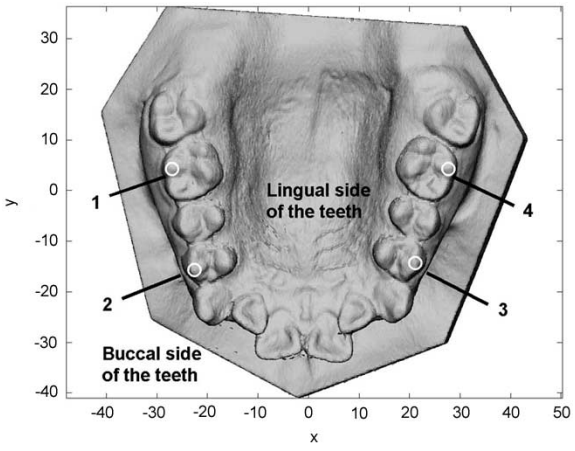

(a)

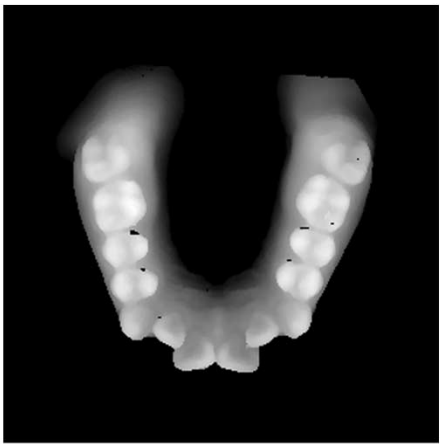

(b)

Fig. 2. (a) Digitized dental cast after alignment and four reference points. (b) Plan-view range image of the digitized dental cast.

need to know the maxillary (upper jaw) and mandibular (lower jaw) arches for assessing the degree of malocclusion [3]. Apart from its clinical use, the dental arch plays an important role in our tooth-segmentation algorithm. Current computer-assisted methods of detecting the arch form require the user to manually select several feature points in the cast image [10] or interactively define the arch [23], [24]. We propose to improve on this with an automated method to detect the tooth-based dental arch.

A. Ridge Detection

From the plan-view range image, we extract orthodontic features such as the incisal edges and cusps. These features appear as local peaks that form ridges (roof edges). Existing detection methods [20], [21] are too dependent on the gradient of the ridge and may fail if the slope is gentle, which is often the case with the cusps of the posterior (back) teeth. We use a new approach, gradient orientation analysis (GOA), to detect both gentle and sharp ridges. Discontinuities in gradient orientation will indicate the presences of local peaks.

Let $h(x,y)$ be a plan-view range image. The gradient of $h(x,y)$ is

$$\nabla h(x,y) = \begin{bmatrix} p(x,y) \\ q(x,y) \end{bmatrix} = \begin{bmatrix} \partial h(x,y)/\partial x \\ \partial h(x,y)/\partial y \end{bmatrix} \tag{1}$$

from which we can compute its orientation

$$\theta(x,y) = \tan^{-1}(q(x,y)/p(x,y)). \tag{2}$$

We ignore the pixels in flat regions where both $p(x,y)$ and $q(x,y)$ are approximately zero. Discontinuities in gradient orientation can be obtained by determining the partial derivatives of the unit gradient vectors $\mathbf{m} = [m_x, m_y]$ as

$$\nabla(\sin\theta(x,y)) = \begin{bmatrix} s_x(x,y) \\ s_y(x,y) \end{bmatrix} = \begin{bmatrix} \partial m_y/\partial x \\ \partial m_y/\partial y \end{bmatrix} \tag{3}$$

$$\nabla(\cos\theta(x,y)) = \begin{bmatrix} c_x(x,y) \\ c_y(x,y) \end{bmatrix} = \begin{bmatrix} \partial m_x/\partial x \\ \partial m_x/\partial y \end{bmatrix} \tag{4}$$

where $\mathbf{m} = [m_x, m_y]$ is given by

$$\begin{cases} m_x(x,y) = p(x,y)/\sqrt{p(x,y)^2 + q(x,y)^2} \\ m_y(x,y) = q(x,y)/\sqrt{p(x,y)^2 + q(x,y)^2} \end{cases}. \tag{5}$$

The Sobel operator is used for computing the partial derivatives. The magnitude of the discontinuities in gradient orientation is obtained as

$$D(x,y) = \sqrt{s_x^2(x,y) + s_y^2(x,y) + c_x^2(x,y) + c_y^2(x,y)}. \tag{6}$$

At this point, both ridges and valleys are detected because they are equally discontinuous in gradient orientation. Ridges are distinguished from valleys by the sign of the Laplacian

$$D_1(x,y) = \begin{cases} D(x,y), & \text{sgn}(\nabla^2 h(x,y)) < 0 \\ 0, & \text{otherwise.} \end{cases} \tag{7}$$

Since we are not interested in the lower portion of the cast, we assign zeros to the points in $D_1(x,y)$ where the gray levels of the corresponding plan-view range image $h(x,y)$ are below 128:

$$D_2(x,y) = \begin{cases} D_1(x,y), & 128 \le h(x,y) \\ 0, & \text{otherwise.} \end{cases} \tag{8}$$

We obtain a binary feature map $M(x,y)$ by thresholding $D_2(x,y)$ with a threshold T given by

$$T = \mu + \sigma \tag{9}$$

where $\mu$and σ denote the mean and the standard deviation of the entire area of $D_2(x,y)$, respectively. Fig. 3(a) shows the ridges extracted from the plan-view range image of Fig. 2(b).

It should be noted that, unlike standard methods of detecting ridges, we use neither the magnitude of the gradient nor the surface normal directly. GOA is capable of detecting ridges irrespective of their gradient magnitude because it focuses solely on the detection of discontinuities in gradient orientation.

B. Two-Step Curve Fitting

The extracted ridge pixels may be used to provide only a crude form of the dental arch. It is necessary to extract and use the orthodontic features that clinically define the dental arch; these are the incisal edges, tips of the canines, and buccal cusps of the posterior teeth. Our procedure employs a two-step curve fitting technique that ensures both stability and flexibility.

In the first step, we apply curve fitting using a third-order polynomial that is robust to over-fitting and yet is sufficiently

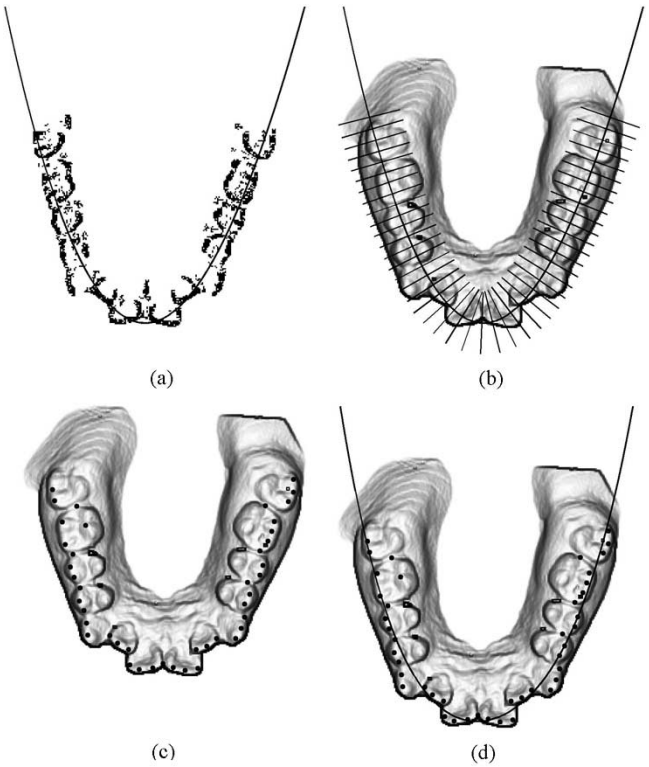

Fig. 3. Two-step curve fitting technique for determining the dental arch. (a) First curve fitting to the extracted ridge points. (b) Inspection spokes. (c) Detected local peaks. (d) Second curve fitting to the local peaks (the dental arch).

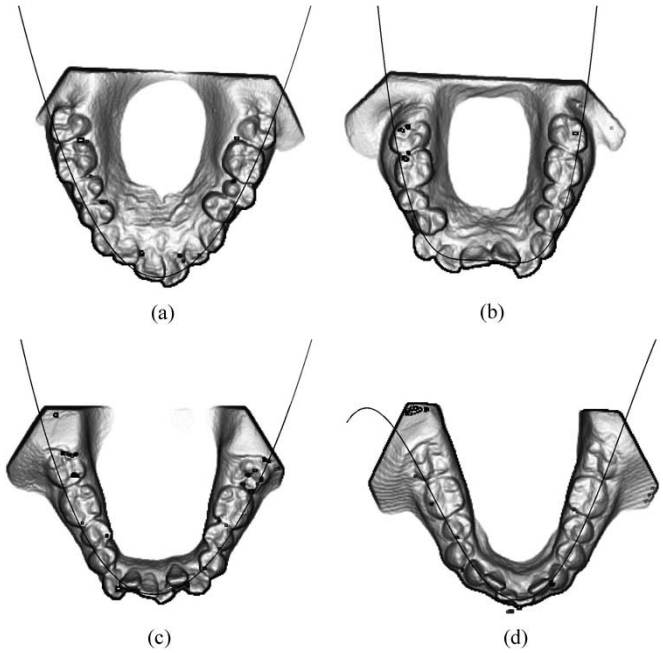

Fig. 4. Various forms of dental arches. (a) Malaligned upper teeth with outwardly inclined incisors. (b) Severely malaligned upper teeth. (c) Malaligned lower teeth. (d) Asymmetrically aligned lower teeth.

flexible to describe the crude form of the arch [Fig. 3(a)]. The best-fitting curve is obtained from weighted least-squares fitting that minimizes the error term, ε

$$\varepsilon = \sum [w(x) \cdot (ax^3 + bx^2 + cx + d - y)]^2. \qquad (10)$$

To reduce the fitting errors around the apex of the dental arch, we have introduced a weight function $w(x)$ that gives greater emphasis to the features of the anterior (front) teeth. A suitable function is

$$w(x) = \frac{1}{|x - x_m| + 1} \qquad (11)$$

where x_m corresponds to the x coordinate of the central pixel in the series of local peaks along the dental arch. We next proceed to set up one-pixel-wide inspection spokes that are oriented perpendicular to the detected arch and search for the pixel with the largest intensity along each spoke [Fig. 3(b)]. The spoke interval is currently set at 1.5 pixels (equivalent to 0.5 mm), which is small enough so as not to miss the orthodontic features. The dots in Fig. 3(c) show the detected local peaks that include the orthodontic features necessary for determining the final dental arch.

In the second step, we find the curve that fits these local peaks by using the weighted least-squares fitting described above with a fourth-order polynomial. This curve is flexible enough to describe the dental arch [Fig. 3(d)] and is in fact commonly used by orthodontists [18], [19]. Unlike symmetrical curves such as the parabola, ellipse or catenary (hyperbolic cosine), higher order polynomials can describe asymmetric curves and do not introduce a bias in the assessment of the dental arches. Fig. 4 shows various forms of dental arches determined by the proposed method.

C. Panoramic Range Image

We generate a panoramic range image by computing the distance between the buccal (outer) surface of the teeth and the reference surface that is defined by extending the detected dental arch (described as a fourth-order polynomial) in the direction perpendicular to the x-y plane. Hence, the reference surface is written as

$$y = ax^4 + bx^3 + cx^2 + dx + e \qquad (12)$$

where a, b, c, d, and e are the coefficients of the polynomial. The plane that is normal to the reference surface at any point (x_0, y_0) on the arch is then given by

$$y = Ax + B = \left(\frac{-1}{4ax_0^3 + 3bx_0^2 + 2cx_0 + d} \right) x + \left(\frac{x_0}{4ax_0^3 + 3bx_0^2 + 2cx_0 + d} + y_0 \right). \qquad (13)$$

The points of intersection (x, y, z) of this plane with the buccal surface of a tooth are obtained by taking those vertices (sample points) that are located within a short distance from the plane. This is necessary since the vertices may not lie exactly on the plane.

The distances from the selected points to the reference surface are subsequently computed and quantized to 256 gray levels to produce the range image. Fig. 8(a) shows a panoramic range image of size 51×245 pixels. The pixel size is 0.3 mm vertically and 0.5 mm horizontally, with one gray level corresponding approximately to 0.06 mm. It is clear that the process of generating the range image does not cause any significant information loss.

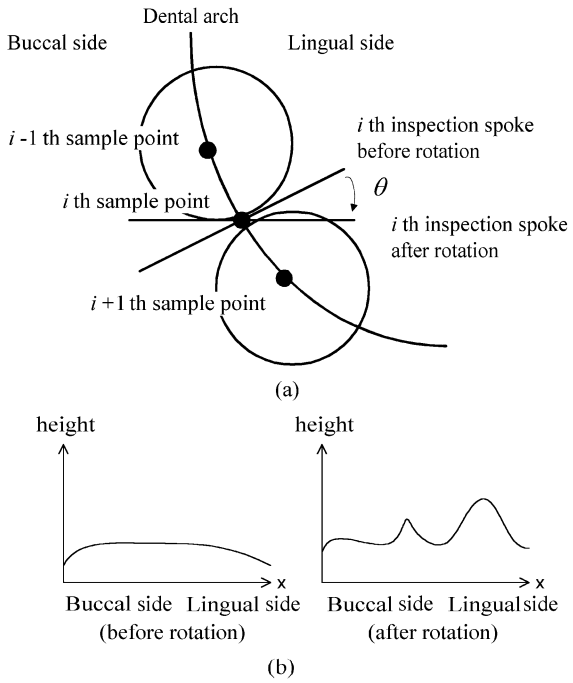

Fig. 5. (a) An inspection spoke and its rotation about the intersection with the dental arch. (b) Cross-sectional profiles along the inspection spoke before and after rotation.

IV. Tooth Segmentation

Tooth segmentation begins with the detection of the interstices between the teeth in the plan-view and panoramic range images. The two results are subsequently combined to obtain the positions and the orientations of the interstices. A complete segmentation also requires the teeth to be separated from the gums.

A. Tooth-Interstice Detection in the Plan-View Range Image

Tooth interstices, which appear as straight grooves or valleys in the plan-view range image, intersect the dental arch at approximately 90 degrees. In earlier work [1], [2], the assumed dental arch is the curved axis of the dental wax imprint, which is not directly related to the arrangement of the teeth. This does not matter if the teeth are well-aligned. However, since we aim to handle dental casts with a variety of malocclusions, it would be appropriate to use the tooth-based dental arch (previous section). We set up inspection spokes along the detected arch and perpendicular to it, and rotate them about their intersections with the arch [Fig. 5(a)]. Two height profiles along the spokes before and after rotation are shown in Fig. 5(b). When an inspection spoke is correctly positioned and oriented with the tooth interstice, the largest height value of the spoke will be smaller than those of other positions and orientations. Therefore, the detection of tooth interstices is reduced to the task of finding significant valleys in a plot of these height values against position (the depth graph).

The detailed procedure for detecting the tooth interstices is as follows.

1) Set up inspection spokes perpendicular to the dental arch with the spoke interval equal to the average spatial resolution of the scanner.

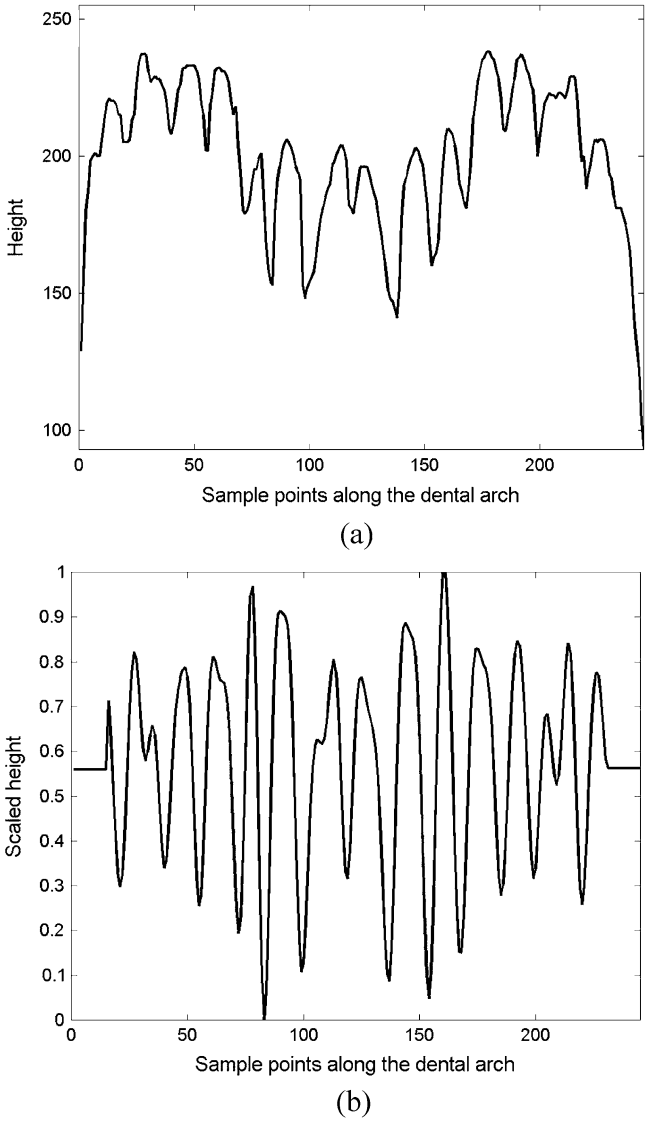

Fig. 6. Depth profile along the dental arch (the depth graph). (a) Before bandpass filtering, $g_1(i)$. (b) After bandpass filtering, $g'_{\mathrm{BPF}}(i)$.

2) Find the depth value of the highest pixel of the ith inspection spoke, i.e., $h_{0,i}$.
3) Rotate the ith inspection spoke by $\pm 10°, \pm 20°, \pm 30°$ about its intersection with the arch.
4) Find the depth value of the highest pixel of each orientation as well, i.e., $h_{10,i}, h_{-10,i}, h_{20,i}, h_{-20,i}, h_{30,i}, h_{-30,i}$.
5) Find the best orientation of the ith spoke by selecting the smallest depth value from the seven values, and store both the depth value and the selected orientation as

$$g_1(i) = \min(h_{0,i}, h_{10,i}, h_{-10,i}, h_{20,i}, h_{-20,i}, h_{30,i}, h_{-30,i}),$$
$$g_2(i) = \text{The angle selected from } 0°, \pm 10°, \pm 20°, \pm 30°.$$

6) Repeat steps 2)–5) for all the inspection spokes.
7) Apply an finite impulse response (FIR) bandpass filter (BPF) to $g_1(i)$ values.

The $g_1(i)$ values (depth graph) show the depth profile along the dental arch [Fig. 6(a)]. We would like to detect the valleys in the depth graph since they correspond to the interstices. To remove the low frequency bias caused by the residual tilt of

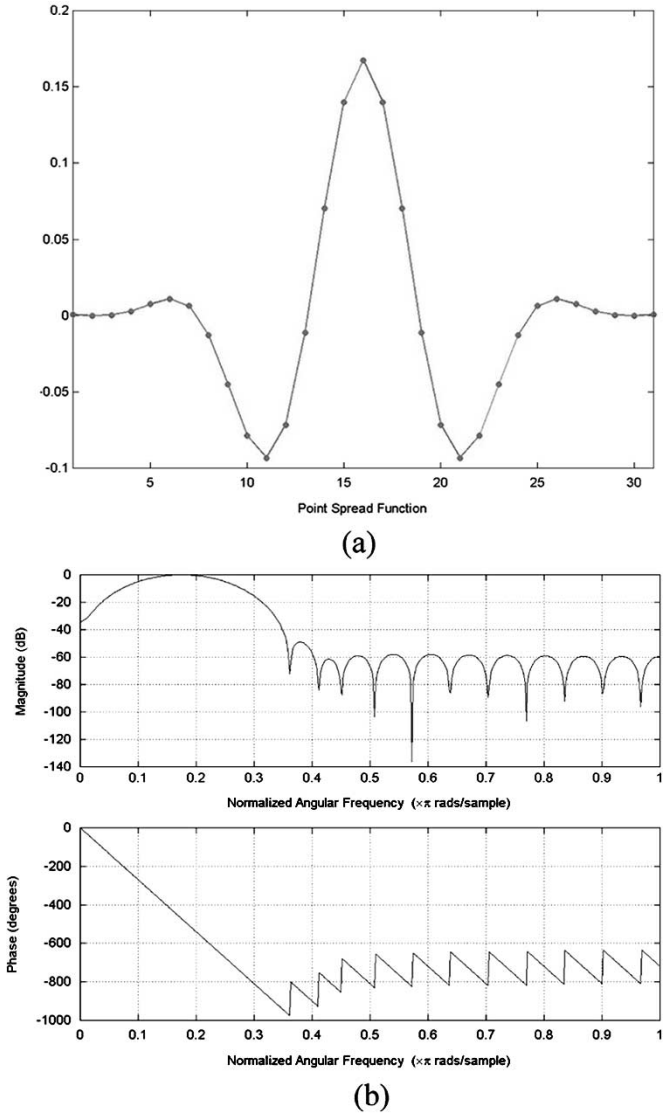

Fig. 7. Designed FIR BPF. (a) Point spread function of the filter and (b) its frequency response.

the cast and the inherent form of the dentition and also high frequency fluctuations due to noise, we first apply an FIR BPF to $g_1(i)$

$$g_{\mathrm{BPF}}(i) = g_1(i) * k(i) \tag{14}$$

where $*$ denotes convolution and $k(i)$ is the point-spread function of the BPF with 31 coefficients [Fig. 7(a)]. The filter was designed by the window method using a Hamming window. The cut-off frequencies (normalized to the Nyquist frequency) at 0.10 and 0.25 correspond to 10 and 4 mm, respectively, which are approximately equivalent to the range of the mesio-distal[7] distances (i.e., front-to-back lengths) of the permanent dentition [Fig. 7(b)]. The depth graph after bandpass filtering is scaled to the range $[0, 1]$ and denoted by $g'_{\mathrm{BPF}}(i)$ [Fig. 6(b)]. For convenience, we express $1-g'_{\mathrm{BPF}}(i)$ as $f_1(i)$ and use it as an indicator of the position of the interstices between the teeth. We can obtain the orientation of the ith interstice by referring to $g_2(i)$.

[7]Anterior, i.e., forward or front of the mouth (*opp*. disto-).

Indicator $f_1(i)$ responds strongly to valleys that are present in the range image; hence, it is efficient for detecting the interstices between posterior teeth and those between malaligned teeth, both of which are relatively deep. A possible weakness is the difficulty in identifying the shallow interstices between incisors. To overcome this problem, we introduce another indicator that is obtained from the panoramic range image.

B. Tooth-Interstice Detection in the Panoramic Range Image

We first employ surface normal analysis (SNA) [22] to detect valleys and ridges (or roof edges) by finding the points where the surface normal changes direction abruptly. We apply SNA in the horizontal direction to detect the vertical valleys formed by the interstices. Let the panoramic range image be $d(i,j)$. The unit surface normal $\mathbf{n}$ is given by

$$\mathbf{n} = \begin{bmatrix} n_i(i,j) \\ n_j(i,j) \\ n_d(i,j) \end{bmatrix} = \frac{1}{\sqrt{1+p^2(i,j)+q^2(i,j)}} \begin{bmatrix} -p(i,j) \\ -q(i,j) \\ 1 \end{bmatrix} \tag{15}$$

where $p(i,j)$ and $q(i,j)$ represent $\partial d(i,j)/\partial i$ and $\partial d(i,j)/\partial j$, respectively. The Sobel operator is again used for estimating the partial derivatives.

We take the d component of the surface normal to be positive since only the surface facing the viewer is visible. Discontinuities in $\mathbf{n}$ will indicate the presence of valleys and ridges in the image. Since we are only interested in detecting vertical valleys here, we search in a horizontal direction (the i direction) for these discontinuities [one-dimensional (1-D) SNA], which are measured by

$$N(i,j) = (\partial n_i(i,j)/\partial i)^2 + (\partial n_j(i,j)/\partial i)^2 + (\partial n_d(i,j)/\partial i)^2. \tag{16}$$

A Sobel mask is used to estimate the horizontal component of the gradient. To separate valleys from ridges, we use the sign of $\nabla^2 d(i,j)$

$$N_{\mathrm{valley}}(i,j) = \begin{cases} N(i,j) & \mathrm{sgn}(\nabla^2 d(i,j)) > 0 \\ 0 & \text{otherwise.} \end{cases} \tag{17}$$

Fig. 8(b) shows $N_{\mathrm{valley}}(i,j)$ of the panoramic range image of Fig. 8(a).

In the second stage, we obtain the vertical projection of $N_{\mathrm{valley}}(i,j)$

$$p(i) = \sum_j N_{\mathrm{valley}}(i,j). \tag{18}$$

The second interstice indicator $f_2(i)$ is $p(i)$ scaled to the range $[0, 1]$ [Fig. 8(c)]. The peaks in $f_2(i)$ can be used to identify the tooth interstices.

Indicator $f_2(i)$ is especially effective when the teeth are well aligned and, thus, the interstices are nearly vertical. It is particularly suitable for detecting the interstices between incisors because they appear as long and prominent peaks. Conversely, $f_2(i)$ may not be so effective if the teeth are severely malaligned. In this case, however, indicator $f_1(i)$ works well (as mentioned above). It should be emphasized that the two indicators complement each other.

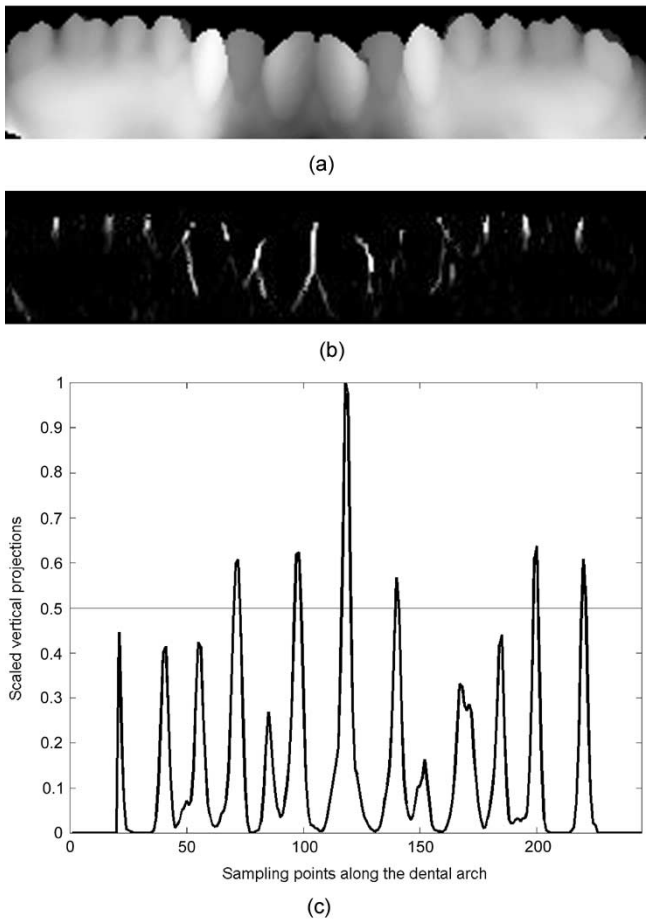

Fig. 8. Detection of the tooth interstices in the panoramic range image. (a) Panoramic range image of the digitized dental cast. (b) Detected vertical valleys. (c) Scaled vertical projections, $f_2(i)$.

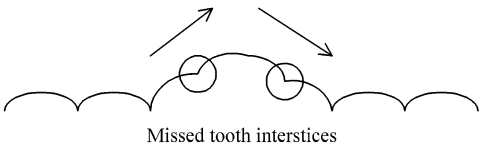

Fig. 9. Cross sectional profile of the panoramic range image.

It is possible to use GOA in place of SNA here, but the latter is considered more reliable in this situation since it detects valleys independently of the viewpoint. Fig. 9 shows the profile of a panoramic range image in which each arc indicates a tooth. The slope increases monotonically to the left of the centre arc and decreases monotonically to the right; GOA will, thus, fail to detect the tooth interstices in the two circles because there is no change in gradient orientation. Such as situation could arise if the dental arch does not fit the arrangement of the teeth very well.

C. Composite Indicator

It is important to note that both tooth-interstice indicators are obtained from the same dental arch and share the same abscissa. The ith value in the depth graph and the ith column of the panoramic range image provide the depth information at the ith sample point on the dental arch. Hence, it is straightforward to combine these two indicators to give a single measure that will serve as a robust indicator of tooth interstices. We require a composite indicator that yields a positive result should any one of the two indicators indicate the presence of an interstice. A simple yet effective measure is the average of $f_1(i)$ and $f_2(i)$

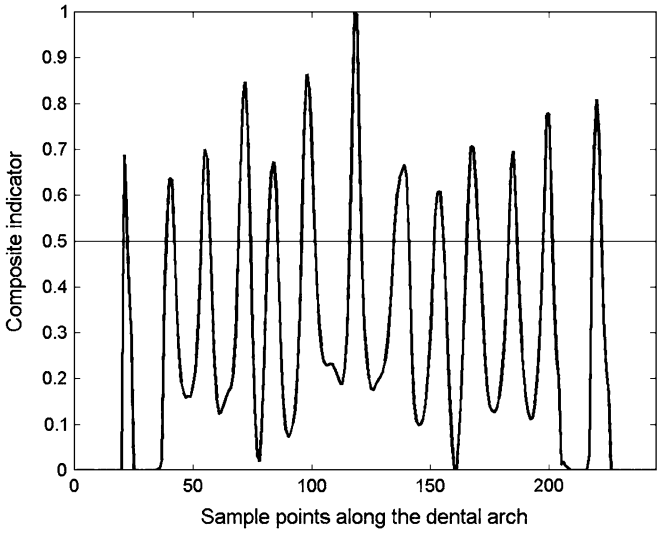

Fig. 10. Composite indicator, $f_c(i)$.

$$f_c(i) = \frac{1}{2}[f_1(i) + f_2(i)] \tag{19}$$

which gives a peak value if at least one of the two indicators successfully detect a tooth interstice. Fig. 10 shows the composite indicator for the dental model of Fig. 2(a).

We determine the location and orientation of the tooth interstices as follows. Suppose we know the number of teeth N (normally 14, except for the wisdom teeth). To find the $N-1$ tooth interstices, we first select the highest $N-1$ peaks in the composite indicator $f_c(i)$ and check their corresponding heights in $f_1(i)$. If a peak value is large (>0.5), we determine the location and orientation of the tooth interstice from the depth graphs $g_1(i)$ and $g_2(i)$, respectively. Local minima are searched for in the depth graph, $g_1(i)$, in the vicinity of the corresponding peaks in the composite indicator $f_c(i)$. When the peak value is low (≤ 0.5) and $f_1(i)$ is not reliable, we determine the location of the tooth interstice using the second indicator $f_2(i)$ and its orientation is considered to be perpendicular to the dental arch. This alternative step is needed when the anterior (front) teeth are well aligned because their interstices are often too small to be detected in the plan view.

With the knowledge about the locations of the two disto-buccal cusps of the first molars (Section II.B), we can limit the number of tooth interstices to be detected along the dental arch between the two cusps to $N-3$. Two more interstices are to be detected outside, but in the vicinity of, the two cusps. In this way, our method does not depend on whether the wisdom teeth are present. When there are only $M(<N-1)$ prominent peaks in the composite indicator, we will attempt to determine M tooth interstices and inform the user of the number of missing interstices, $N-M-1$.

Though we assume that N is known, it is a trivial matter to allow for missing teeth. A deep and wide valley in the depth graph or panoramic range image would signal clearly that one

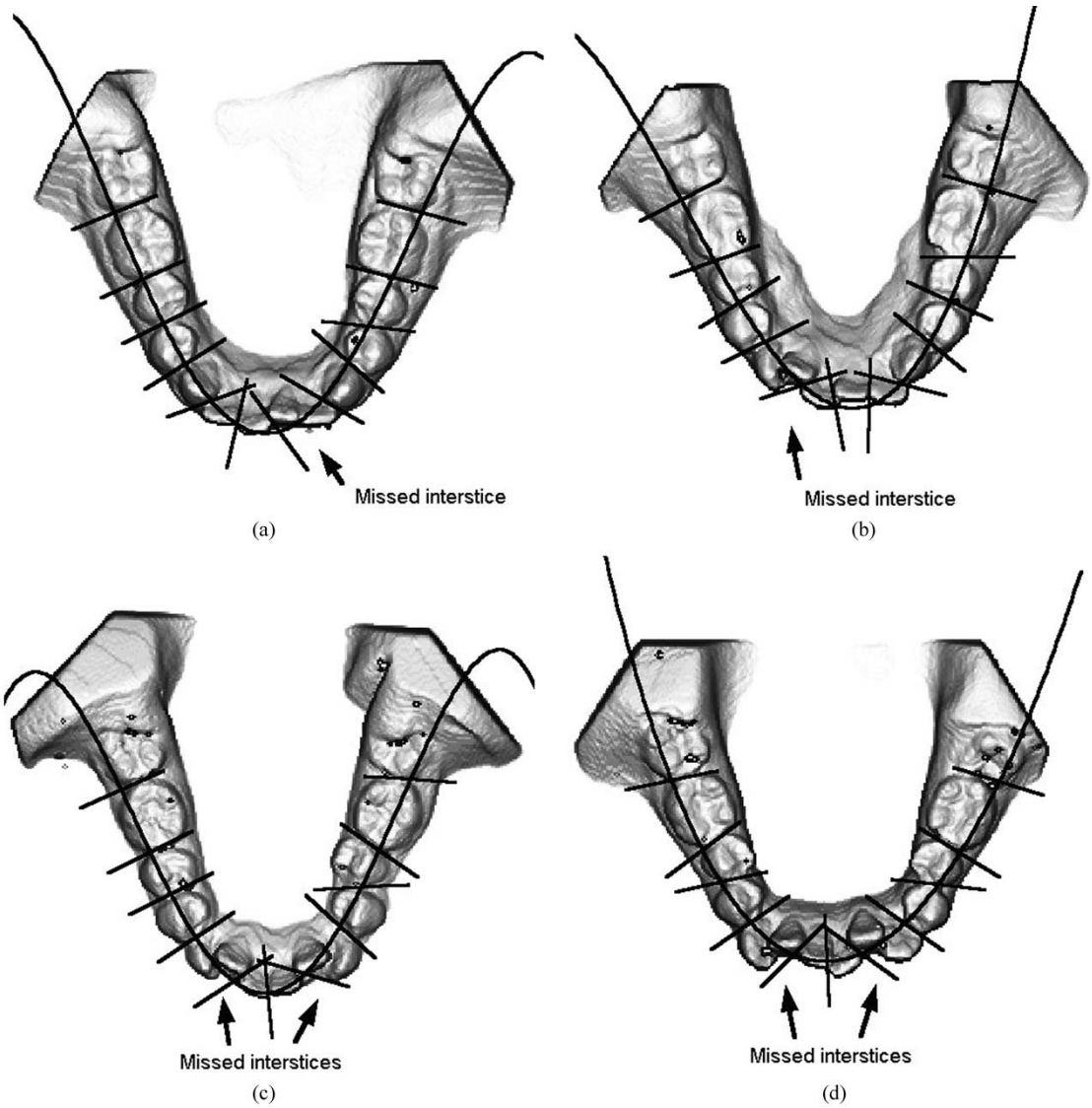

Fig. 11. Detected dental arches and tooth interstices. (a) Mandible of Class I with bimaxillary proclination. (b) Mandible of Class I with bimaxillary proclination. (c) Mandible of Class II division 1. (d) Mandible of Class II division 1.

TABLE I
ORIENTATION DEVIATIONS OF THE DETECTED TOOTH INTERSTICES WITH RESPECT TO THE GROUND TRUTH

	Anterior Teeth	Posterior Teeth	Average
Maxilla	5.7°	3.6°	4.7°
Mandible	6.2°	4.6°	5.4°
Average	5.9°	4.1°	5.1°

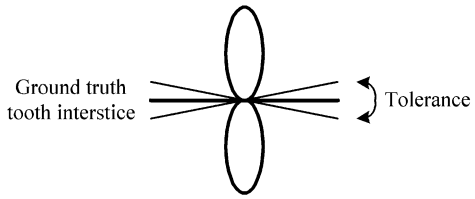

Fig. 12. Tolerance in interstice orientation.

or more teeth are missing, with statistical knowledge of tooth sizes employed to determine the actual number.

D. Separation of the Teeth From the Gum

The teeth need to be separated from the gums in applications that require modeling or designing of tooth crowns [4]–[7], while the extracted gum portion would be of use in applications that require measurements to be made of the gum. The border between the teeth and the gums (the gum margin) appears as a valley at each column of the panoramic range image. The valley can be located by finding the pixel where discontinuity in surface normal is the largest at each column of the image. Since the sharpness of the valleys varies widely from the anterior teeth (shallow) to the posterior teeth (deep), we employ a family of derivative-operators such as $[1, 0, -1]^T$, $[1, 0, 0, 0, -1]^T$, and $[1, 0, 0, 0, 0, 0, -1]^T$ for computing the discontinuities in surface normals (using the 1-D SNA).

In every column of the image, we will obtain three candidate valley pixels. They are ranked according to their reliability,

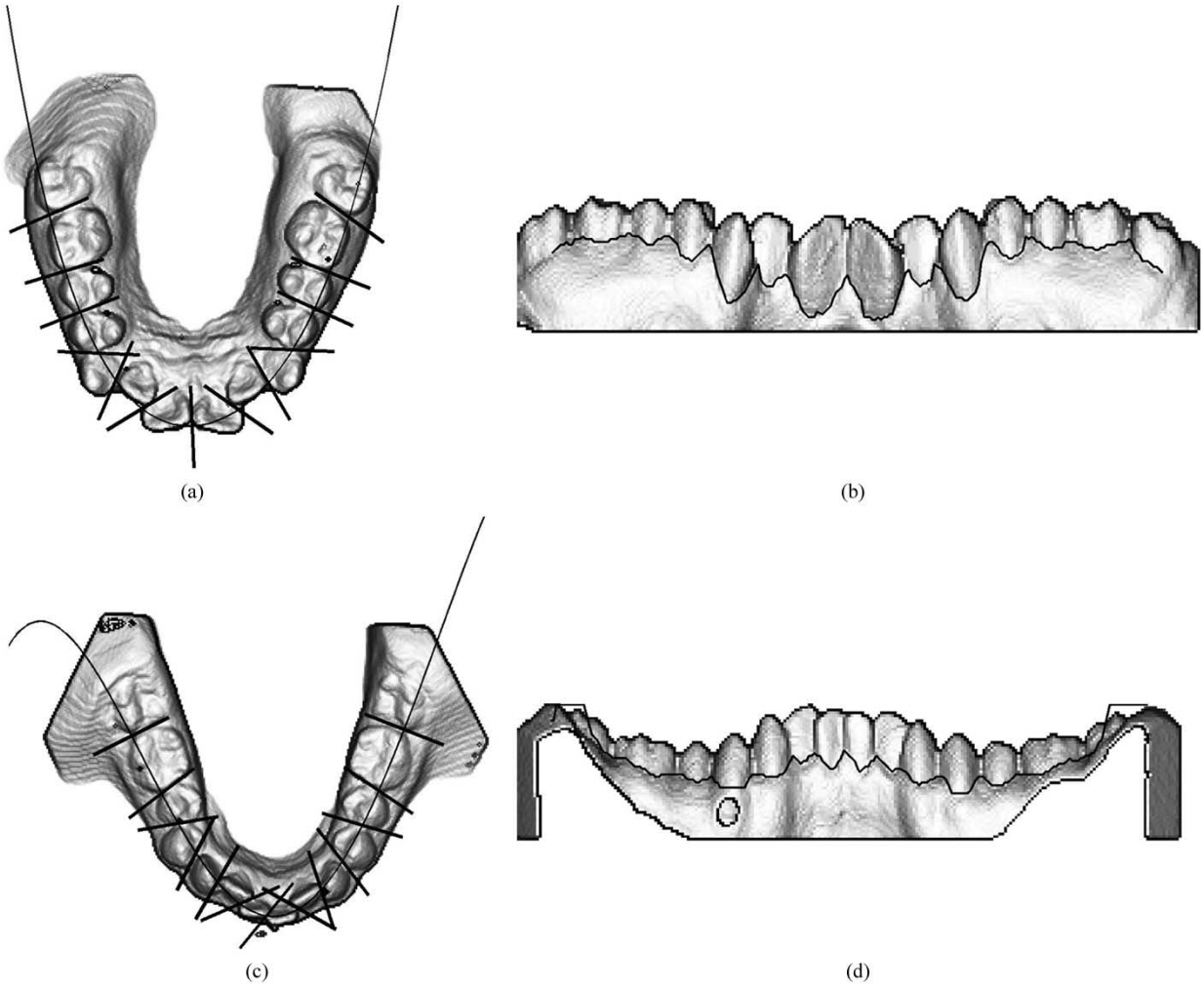

Fig. 13. Segmented teeth. (a) Segmented maxilla of Class I with bimaxillary proclination in the plan view. (b) Same cast in the panoramic view. (c) Segmented mandible of Class II division 1 in the plan view. (d) Same cast in the panoramic view.

i.e., the magnitude of the derivative. The gum border is initially drawn by connecting the most reliable candidates and its smoothness evaluated by

$$s(i) = |t_j(i-1) - 2 \cdot t_j(i) + t_j(i+1)| \qquad (20)$$

where i denotes the index of a column of the image and $t_j(i)$ the row of the jth candidate $(j = 1, 2, 3)$ of the ith column. If $s(i)$ exceeds a preset value, this valley pixel is considered too isolated from its neighbors and replaced with the second candidate (and the third, if necessary) pixel of the column. In the unlikely event that all three candidates at a column fail to satisfy the smoothness criterion, we interpolate the border pixel. Fig. 13(b) and (d) shows two examples of detected gum borders.

V. Results and Discussion

We have tested our tooth-segmentation algorithm on 34 dental casts with various types of malocclusions, namely, Class I,[8] Class I with bimaxillary proclination,[9] Class II division 1,[10] and Class II division 2.[11] Each class has 8 casts comprising 4 maxillas (upper jaw) and 4 mandibles (lower jaw). Two more casts of unknown class, a maxilla and a mandible, were also used. Visual inspection was used to evaluate the segmentation results. The method correctly detected all the 390 tooth interstices in 30 casts and missed 6 tooth interstices of the anterior teeth in the remaining 4 (Fig. 11), a failure rate of 1.4%. There are two causes of unsuccessful detection

- *Limited Resolution of the Scanner:* When the valley formed by two adjoining teeth is extremely fine [Fig. 11(a)], it will not appear in both plan and panoramic views.
- *Severe Overlap of Two Adjoining Teeth:* When two adjoining teeth overlap with each other [Fig. 11(b)–(d)], they do not form a valley in the panoramic view, which renders the second indicator ineffective. If the contact surface between the two neighboring teeth is highly curved, the straight inspection spoke cannot fit into the interstice

[8]Class I malocclusion has the normal molar relationship but the incorrect line of occlusion.

[9]Both the upper and lower incisors are proclined toward the lips.

[10]Class II, division 1, malocclusion has the lower molar placed behind the upper molar, and the upper incisors are inclined outward.

[11]Class II, division 2, malocclusion has the lower molar placed behind the upper molar, and the upper incisors are inclined inward.

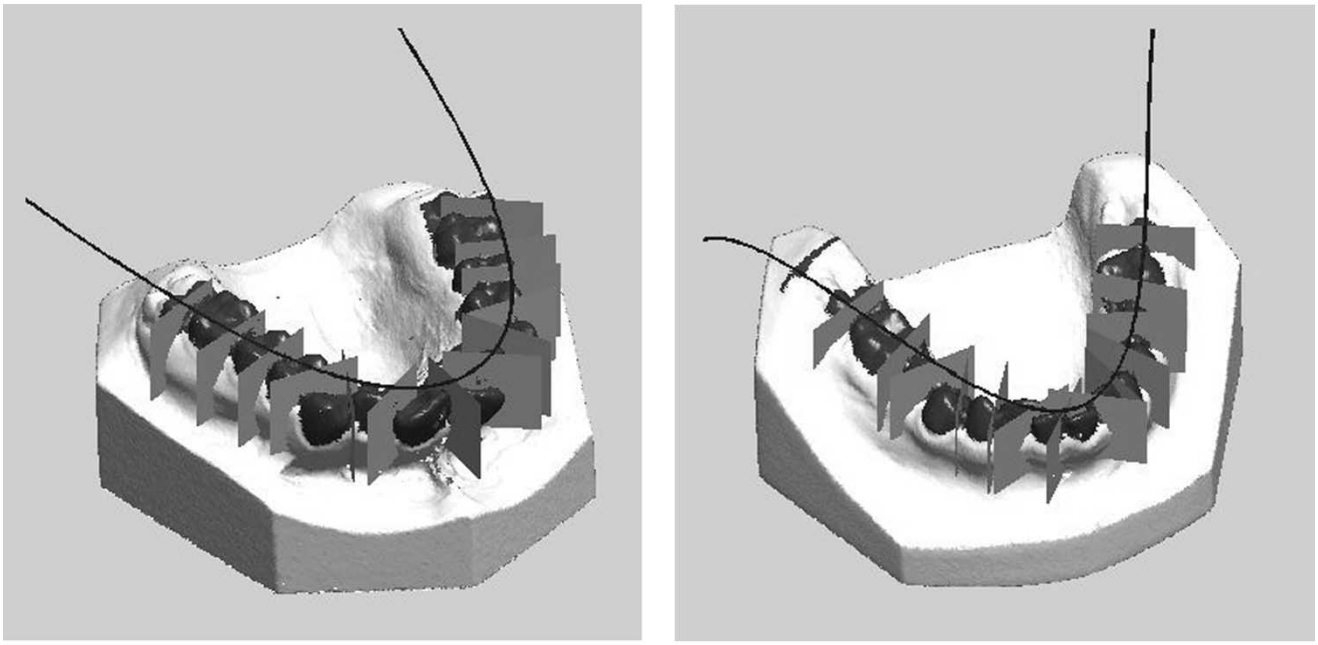

(a) (b)

Fig. 14. Three-dimensional presentation of the segmented teeth. (a) Segmented maxilla of Class I with bimaxillary proclination [corresponding to the dental cast of Fig. 13(a) and (b)]. (b) Segmented mandible of Class II, division 1 [corresponding to the dental cast of Fig. 13(c) and (d)].

at any orientation, thus causing the first indicator to also be ineffective.

What is significant, however, is that the system does not give any false detections even in such a situation but will notify the user of the number of undetected interstices. The orientations of the detected tooth interstices are evaluated by comparing with those specified by an orthodontist. The deviations in the two orientations are summarized in Table I. The average deviation is about 5°, which is equal to the quantization error as we rotate the inspection spoke every 10°. In addition, it should be noted that there is some tolerance in defining the orientation of a tooth interstice (Fig. 12).

The proposed method successfully delineated the border between the teeth and gums in every cast. The overall result is noteworthy, considering the fact that we have used casts with malocclusions that are commonly encountered in orthodontic treatments. Fig. 13 shows two sets of tooth segmentation results in both plan and panoramic views. Fig. 13(a) and (b) shows the segmented upper teeth of a Class I malocclusion with bimaxillary proclination and Fig. 13(c) and (d) shows the lower teeth of a Class II division 1 malocclusion. The segmentation results can be back-projected to the digitized cast to give a 3-D presentation of the segmentation (Fig. 14).

We discuss the features of our approach with respect to the two cases of well-aligned teeth and malaligned teeth.

- *Well-aligned case.* When the teeth are well aligned, it is often difficult to identify the interstices between incisors in the plan view while they form clear vertical valleys in the panoramic view. Fig. 15 demonstrates the importance of using both indicators. Three tooth interstices between the incisors are missing (or too low) in the first indicator [Fig. 15(a)]. In contrast, the second indicator shows the three peaks clearly [Fig. 15(b)]. These peaks are so prominent that the tooth interstices missing in the first indicator are recovered in the composite indicator [Fig. 15(c)], leading to the successful detection of the interstices [Fig. 15(d)].
- *Malaligned case.* When the teeth are malaligned, their interstices do not always form valleys in the panoramic view, resulting in lower reliability of the second indicator. The first indicator is effective because interstices between malaligned teeth generally appear as deep valleys in the plan view. This situation can be seen in Fig. 16, where the 14 teeth result in 13 tooth interstices. There is one missing peak in the second indicator [Fig. 16(b)] caused by severe tooth malalignment. However, the first indicator has the highest peak at the same position [Fig. 16(a)], and 13 peaks can be clearly seen in the composite indicator [Fig. 16(c)]. The tooth interstices in this case are successfully detected [Fig. 16(d)].

As confirmed by our experiments, the first indicator (obtained from the plan view) could be unreliable in detecting interstices between well-aligned incisors, but is quite tolerable to malaligned teeth. The second indicator (obtained from the panoramic view), on the other hand, may be unreliable when the teeth are malaligned, but works very well for well-aligned teeth. Therefore, these two indicators work in a complementary manner by covering for each other's weakness. Consequently, the method has achieved a high success rate in segmenting teeth with a variety of malocclusions.

VI. Conclusion and Future Work

This paper has presented an automated method for tooth segmentation of dental study models representing a variety of malocclusions. The study model is digitized into triangular mesh data by a laser scanner. Instead of processing the 3-D mesh

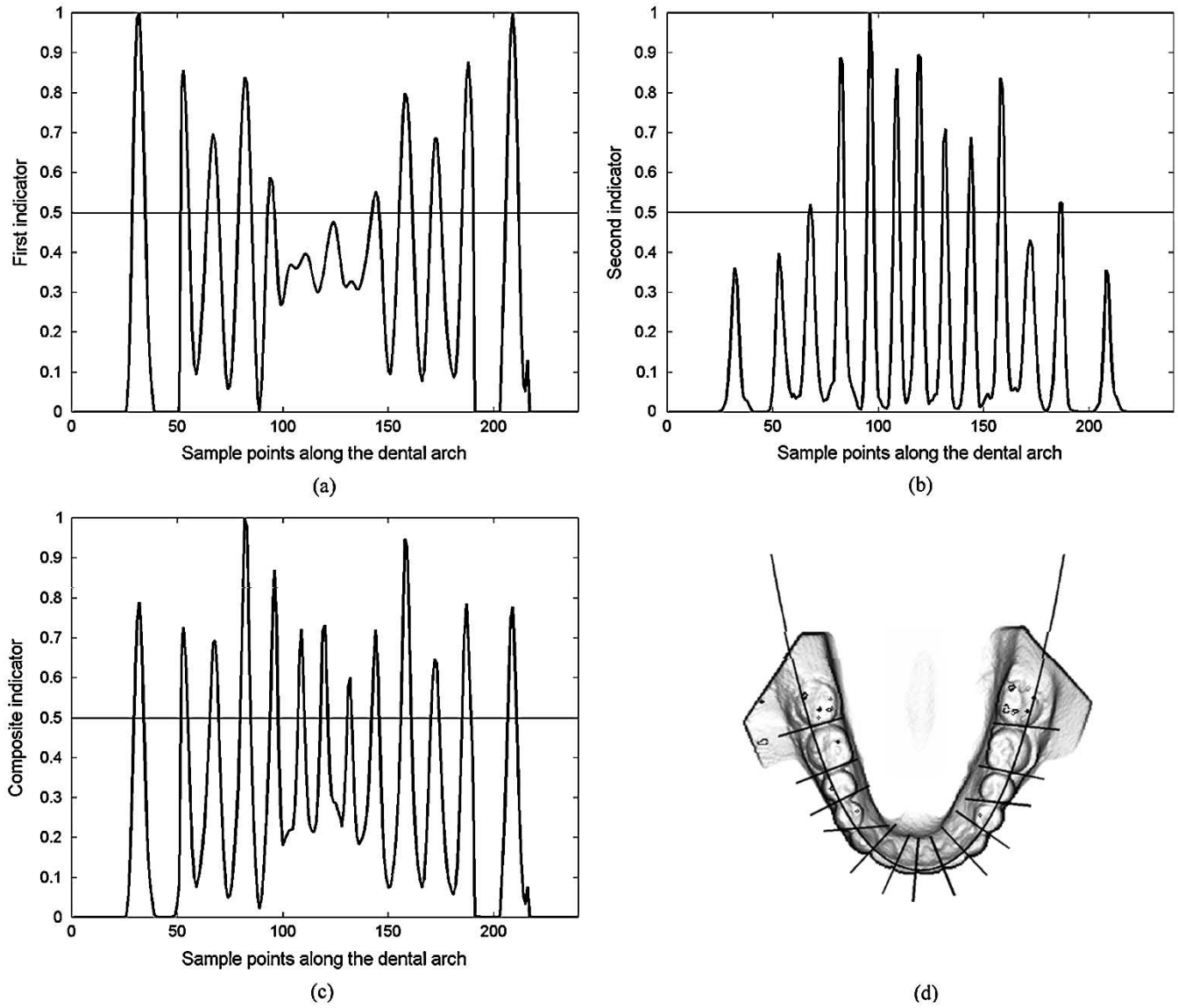

Fig. 15. Integration of the two indicators in an well-aligned case. (a) First indicator. (b) Second indicator. (c) Composite indicator. (d) Detected tooth interstices.

model directly, we have devised algorithms that are applied to the range images generated from the mesh data.

We first compute a plan-view range image of the model and determine the dental arch based on the arrangement of the teeth. Since this tooth-based dental arch passes through orthodontic features irrespective of the malalignment of the teeth, it greatly relaxes the restriction on the models that the method can deal with. Using the dental arch as the reference, we next compute a panoramic range image of the model, which describes the distance between the reference and the buccal surface of the teeth. The pixel size and the gray levels of these two range images are determined by the spatial and depth resolutions of the laser scanner. In this way, the details of the model necessary for tooth segmentation are efficiently transferred from an irregular mesh domain to a regular image domain.

Several benefits accrue by conversion of the 3-D mesh data into the regular data structure represented by the range image. It allows the application of mathematical operations such as convolution and the employment of robust techniques such as GOA and SNA for extracting image features. The advantage of GOA lies in its ability to detect ridges/valleys irrespective of their gradient magnitude, which is particularly important since the dental features include sharp incisal edges as well as cusps with gentle slopes. The 1-D version of SNA was used for detecting both vertical valleys (tooth interstices) and horizontal valleys (gum margin). Hence, a complex 3-D tooth segmentation problem is greatly simplified by employing two range images.

For effective detection of tooth interstices, both range images are employed, with the results from both views subsequently combined to obtain the locations and the orientations of the interstices. The plan-view range image plays an important role in the detection of the interstices between the posterior (back) teeth and also between malaligned teeth. The panoramic range image has an important complementary role as it is suited to the detection of interstices between well aligned teeth, particularly the anterior (front) teeth. The teeth are separated from the gums in the panoramic range image. A validation test on 34 dental models with a variety of malocclusions shows that the method is robust and accurate.

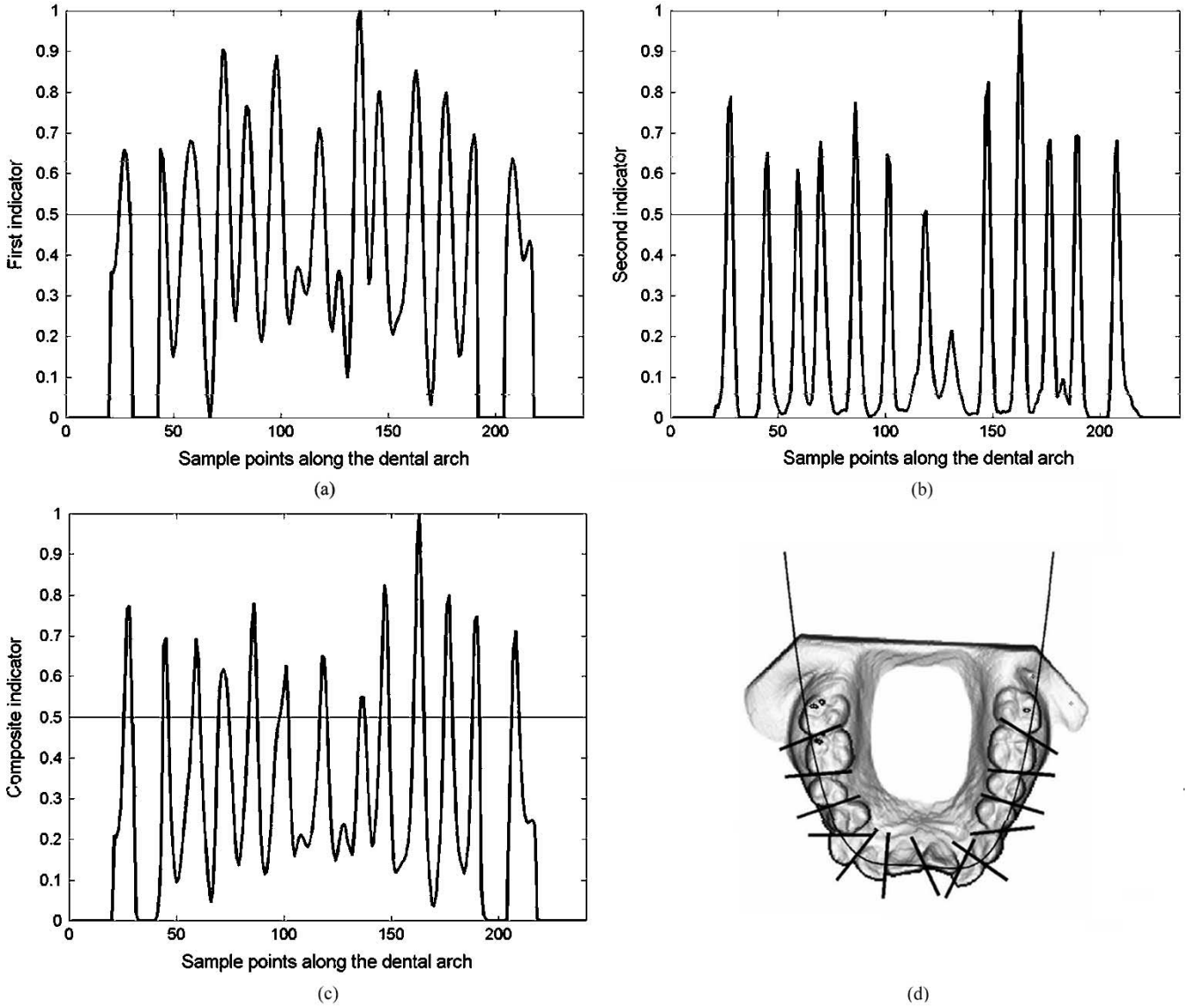

Fig. 16. Integration of the two indicators in a malaligned case. (a) First indicator. (b) Second indicator. (c) Combined indicator. (d) Detected tooth interstices.

Our method is fully automatic once the dental study model has been aligned to a standard orientation. Alignment itself may be automated by first detecting the base of the dental model, which appears as a flat surface. From the corresponding plan-view range image, GOA can be used to extract the ridges. Then the cast can be aligned such that the ridges are approximately at the same height and the U-shaped ridge distribution becomes symmetric.

We intend to further improve the success rate of detecting the tooth interstices. When the present method fails to detect a tooth interstice, a curved inspection spoke may be employed. To make the second indicator more sensitive to malaligned teeth, we will test the use of a line-fitting technique in place of the vertical projection. We will also study an optimal combination of the two indicators that can vary adaptively according to the arrangement of the teeth. Furthermore, the application of our surface segmentation method to volumetric data will be investigated, for example, extending GOA into three dimensions for analyzing CT and MR images.

REFERENCES

[1] D. Laurendeau, L. Guimond, and D. Poussart, "A computer-vision technique for the acquisition and processing of 3-D profiles of dental imprints: an application in orthodontics," *IEEE Trans. Med. Imag.*, vol. 10, pp. 453–461, Sept. 1991.

[2] J. Cote, D. Laurendeau, and D. Poussart, "A multi-operator approach for the segmentation of 3-D images of dental imprints," *Advances in Machine Vision, Strategies and Applications*, pp. 343–360, 1992.

[3] M. Mokhtari and D. Laurendeau, "Feature detection on 3-D images of dental imprints," in *Proc. IEEE Workshop Biomedical Image Analysis*, June 1994, pp. 287–296.

[4] D. Paulus, M. Wolf, S. Meller, and H. Niemann, "Three-dimensional computer vision for tooth restoration," *Med. Image Anal.*, vol. 3, no. 1, pp. 1–19, 1999.

[5] E. D. Rekow, A. G. Erdman, D. R. Riley, and B. Klamecki, "CAD/CAM for dental restorations—Some of the curious challenges," *IEEE Trans. Biomed. Eng.*, vol. 38, pp. 314–318, Apr. 1991.

[6] K. Myszkowski, V. V. Savchenko, and T. L. Kunii, "Computer modeling for the occlusal surface of teeth," in *Proc. Computer Graphics Int.*, 1996, pp. 191–198.

[7] T. Hayashi, J. Tsuchida, and K. Kato, "Semi-automatic design of tooth crown using a 3-D dental CAD system, Vocs-1B," in *Proc. 22th Ann. Int. Conf. IEEE Engineering in Medicine and Biology Society*, July 2000, pp. 565–566.

[8] K. Yamamoto, S. Hayashi, H. Nishikawa, S. Nakamura, and T. Mikami, "Measurement of dental cast profile and three-dimensional tooth movement during orthodontic treatment," *IEEE Trans. Biomed. Eng.*, vol. 38, pp. 360–365, Apr. 1991.

[9] N. Motohashi and T. Kuroda, "A 3D computer-aided design system applied to diagnosis and treatment planning in orthodontics and orthognathic surgery," *Eur. J. Orthodont.*, vol. 21, pp. 263–274, 1999.

[10] J. H. Chuah, S. H. Ong, T. Kondo, K.W.C. Foong, and T. F. Yong, "3D space analysis of dental models," in *Proc. SPIE Int. Symp. Medical Imaging 2001*, San Diego, CA, Feb. 2001.

[11] V. Mok, S. H. Ong, K. W. C. Foong, and T. Kondo, "Pose estimation of teeth through crown-shape," in *Proc. SPIE Int. Symp. Medical Imaging 2001*, San Diego, CA, Feb. 2002.

[12] S. M. Yamany, A. A. Farag, and N. A. Mohamed, "Orthodontics measurements using computer vision," in *Proc. 20th Ann. Int. Conf. IEEE Engineering in Medicine and Biology Society*, vol. 20, 1998, pp. 536–539.

[13] S. M. Yamany and A. R. El-Bialy, "Efficient free-form surface representation with application in orthodontics," *Proc. SPIE*, vol. 3640, pp. 115–124, Jan. 1999.

[14] A. A. Goshtasby, S. Nambala, W. G. deRijk, and S. D. Campbell, "A system for digital reconstruction of gypsum dental casts," *IEEE Trans. Med. Imag.*, vol. 16, pp. 664–674, Oct. 1997.

[15] A. A. Goshtasby, "Three-dimensional model construction from multiview range images: Survey with new results," *Pattern Recogn.*, vol. 31, no. 11, pp. 1705–1714, 1998.

[16] Y. Hirogaki, T. Sohmura, H. Satoh, J. Takahashi, and K. Takada, "Complete 3-D reconstruction of dental cast shape using perceptual grouping," *IEEE Trans. Med. Imag.*, vol. 20, pp. 1093–1101, Oct. 2001.

[17] S. M. Yamany, A. A. Farag, D. Tasman, and A. G. Farman, "A 3-D reconstruction system for the human jaw using a sequence of optical images," *IEEE Trans. Med. Imag.*, vol. 19, pp. 538–546, May 2000.

[18] V. F. Ferrario, C. Sforza, A. Miani, Jr., and G. Tartaglia, "Mathematical definition of the shape of dental arches in human permanent healthy dentitions," *Eur. J. Orthodont.*, vol. 16, pp. 287–294, 1994.

[19] S. J. Rudge, "Dental arch analysis: Arch form, a review of the literature," *Eur. J. Orthodont.*, vol. 3, pp. 279–284, 1981.

[20] P. J. Besl and R. C. Jain, "Segmentation through variable-order surface fitting," *IEEE Trans. Pattern Anal. Machine Intell*, vol. 10, pp. 167–192, Mar. 1988.

[21] A. Hoover, G. Jean-Baptiste, X. Jiang, P. J. Flynn, H. Bunke, D. B. Goldgof, K. Bowyer, D. W. Eggert, A. Fitzgibbon, and R. B. Fisher, "An experimental comparison of range image segmentation algorithms," *IEEE Trans. Pattern Anal. Machine Intell*, vol. 18, pp. 673–689, July 1996.

[22] N. Yokoya and M. D. Levine, "Range image segmentation based on differential geometry: A hybrid approach," *IEEE Trans. Pattern Anal. Machine Intell.*, vol. 11, pp. 643–649, June 1989.

[23] J. Brief, S. Hassfeld, W. Stein, R. Krempien, and J. Muehling, "Clinical evaluation of patient misalignment during CT scans for computer assisted implantology—A new approach for compensation," in *Proc. 16th Int. Congr. Computer-Aided Radiology and Surgery, CARS2002*, Paris, France, 2002, pp. 943–946.

[24] K. Schicho, A. Wagner, and R. Ewers, "Computer aided navigation and interactive teleconsultation in dental implantology," in *Proc. 16th Int. Congr. Computer-Aided Radiology and Surgery, CARS2002*, Paris, France, 2002, pp. 975–980.